Hydrometeorological Response of the Modeled North American Monsoon to Convective Parameterization

DAVID J. GOCHIS, W. JAMES SHUTTLEWORTH, AND ZONG-LIANG YANG

Department of Hydrology and Water Resources, The University of Arizona, Tucson, Arizona

(Manuscript received 13 November 2001, in final form 26 August 2002)

ABSTRACT

This paper describes the second part of a study to document the sensitivity of the modeled regional moisture flux patterns and hydrometeorological response of the North American monsoon system (NAMS) to convective parameterization. Use of the convective parameterization schemes of Betts–Miller–Janjic, Kain–Fritsch, and Grell was investigated during the initial phase of the 1999 NAMS using version 3.4 of the fifth-generation Pennsylvania State University–National Center for Atmospheric Research (PSU–NCAR) Mesoscale Model (MM5) running in a pseudoclimate mode. Substantial differences in both the stationary and transient components of the moisture flux fields were found between the simulations, resulting in differences in moisture convergence patterns, precipitation, and surface evapotranspiration. Basin-average calculations of hydrologic variables indicate that, in most of the basins for which calculations were made, the magnitude of the evaporation-minus-precipitation moisture source/sink differs substantially between simulations and, in some cases, even the sign of the source/sink changed. There are substantial differences in rainfall–runoff processes because the basin-average rainfall intensities, proportion of rainfall from convective origin, and the runoff coefficients differ between simulations. The results indicate that, in regions of sustained, deep convection, the selection of the subgrid convective parameterization in a high-resolution atmospheric model can potentially have a hydrometeorological impact in regional analyses, which is at least as important as the effect of land surface forcing.

1. Introduction

Water resources are highly stressed in many areas influenced by the North American monsoon system (NAMS), and this provides impetus for developing and testing seasonal hydrometeorological prediction systems in this region. Communities in the southwestern United States and northern Mexico directly or indirectly rely on rains attributed to the NAMS for their social well-being and economic livelihood (e.g., Morehouse et al. 2000). Figure 1 shows the monthly percentage of mean annual discharge for seven river systems in the region: U.S. streamflow data are from the United States Geological Survey (USGS); Mexican data are from the Bancos Nacional de Datos de Aguas Superficiales archive, BANDAS (1998). The periods of record do not all overlap due to gaps in the data. Proceeding southward from the southern Colorado Plateau into central-west Mexico, summer precipitation generates more annual streamflow than winter precipitation or snowmelt.

This paper reports the second part of a study to investigate the sensitivity of simulated North American monsoon (NAM) circulation to different model representations of convection. The fifth-generation Pennsylvania State University–National Center for Atmospheric Research (PSU–NCAR) Mesoscale Model (MM5) was run three times in a nested-domain, regional climate mode with representation of subgrid convection in the internal 30-km domain made using the Betts–Miller–Janjic (BMJ), Kain–Fritsch (KF), and the Grell (GR) schemes, respectively. The first part of the study (Gochis et al. 2002, hereafter referred to as G1) documented the sensitivity of modeled precipitation, column-integrated precipitable water, surface air and dewpoint temperatures, and atmospheric stability to these three different representations of subgrid convection. The following are the main conclusions from G1.

- There are differences in both the time-integrated thermodynamic and circulation structures of the simulated July 1999 NAM atmosphere when different convective parameterization schemes (CPSs) are used, with markedly different regional circulation patterns revealed in the vertical velocity and low-level divergence fields.
- Differences in the circulation fields contribute to very different modeled fields of July-average column-integrated precipitable water, but errors in the modeled surface dewpoint temperature are greater in the northern monsoon region than elsewhere, regardless of the convective scheme used.

Corresponding author address: W. James Shuttleworth, Department of Hydrology and Water Resources, The University of Arizona, Harshbarger Building 11, Tucson, AZ 85721.
E-mail: shuttle@hwr.arizona.edu

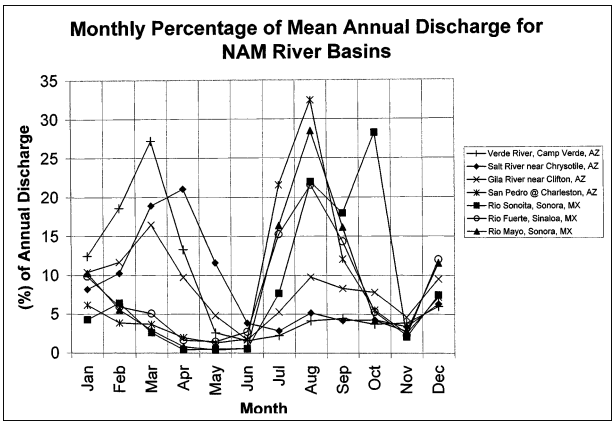

FIG. 1. Monthly percent of mean annual discharge volume for selected basins in the southwest United States and northwest Mexico.

- All of the model simulations reproduced a precipitation maximum along the western slope of the Sierra Madre Occidental, but the root-mean-square errors and bias relative to rainfall and surface climate observations were substantial and showed strong regional dependency in each simulation.

The present study extends G1 by examining the difference in the hydrological response modeled in the three climate simulations with different parameterizations of convection.

Several authors have examined the atmospheric branch of the NAMS (e.g., Schmitz and Mullen 1996; Higgins et al. 1997; Berbery 2001; Anderson and Roads 2001; Anderson et al. 2000a) using analyzed or reanalyzed data. Using European Centre for Medium-Range Weather Forecasts (ECMWF) reanalysis data at T106 spectral resolution, Schmitz and Mullen (1996) showed that moisture flux into the core NAM region of western Mexico and the southwestern United States is attributable to low-level stationary components traveling up the Gulf of California (GoC), while larger-scale circulation around the summertime continental anticyclone over the southeastern United States is subsequently responsible for transporting the moisture (generated by deep convection over the Sierra Madre Occidental) from midtropospheric levels, northward into the southwestern United States. The transient component of the moisture flux, although comparatively small, comprises a significant portion of the total moisture flux emanating from the northern GoC. Regional estimates of moisture convergence also reveal that land regions act as moisture sinks and the waters of the Gulf of California, the eastern Pacific, and the Gulf of Mexico are moisture sources.

Using analyses and short-term forecasts from the Eta Data Assimilation System (EDAS) at 40-km resolution, Berbery (2001) also found large and persistent divergence of moisture over the northern GoC, along with increased transient moisture flux out of this region. However, there were substantial differences in the direction of the integrated moisture flux over the GoC between the analyses of Schmitz and Mullen (1996) and Berbery (2001). According to Berbery, these differences in flux fields are due to differences in the ''mesoscale nature'' of the analysis products and are attributable to the higher-resolution topography used in the EDAS model. Such mesoscale features appear also to be well captured in recent modeling studies by Anderson et al. (2000a,b), who documented the diurnal behavior of the GoC low-level jet as well as the occurrence of gulf surges.

Determining the underlying causes for differences between the previously mentioned analyses is difficult because the analyses were made for different time periods with markedly different modeling systems and different spatial resolutions. In the present study, one potential cause of differences was isolated by making otherwise identical simulations with different representations of subgrid convection. A further important dissimilarity between the present study and the earlier studies of Berbery (2001) and Schmitz and Mullen (1996) is that, in this study, the MM5 model is operated in free-running regional climate mode rather than in assimilation mode. The forcing is provided by prescribing lateral boundary conditions and sea surface temperature, and the model evolves a climate in the modeled domain that is a nonlinear function of the boundary conditions and model physics parameterizations (Giorgi and Mearns 1999). As previously stated, this study extends G1 with focus on fields of hydrologic importance, specifically, patterns of moisture convergence, net surface moisture exchange, precipitation characteristics, and surface runoff. Section 2 describes the model setup and analysis methods used; section 3 gives the results, which are then discussed in section 4. Section 5 provides concluding remarks.

2. Model and analysis methods

a. Model setup

The model setup is described briefly below, but the reader is referred to G1 for greater detail. Three similar simulations were made using version 3.4 of the PSU–NCAR MM5 (Grell et al. 1994), each with two-domain configurations: the coarse domain resolution was 90 km and the fine domain 30 km (see Fig. 1 in G1). The coarse domain approximately covers the region shown in Fig. 2, that is, 10°–45°N and 85°–125°W, and the internal domain is shown as a box in this figure. Initial tests showed sensitivity to model configuration (especially the winds over the Gulf of California), and the size and location of the internal domain boundaries were chosen recognizing this. However, some remnant sensitivity may still be present in the results. The model specified 23 vertical levels in both the coarse and fine resolution domains. Terrain heights (which were interpolated in each domain by MM5 preprocessing routines) differed between the grids, which could potentially also affect

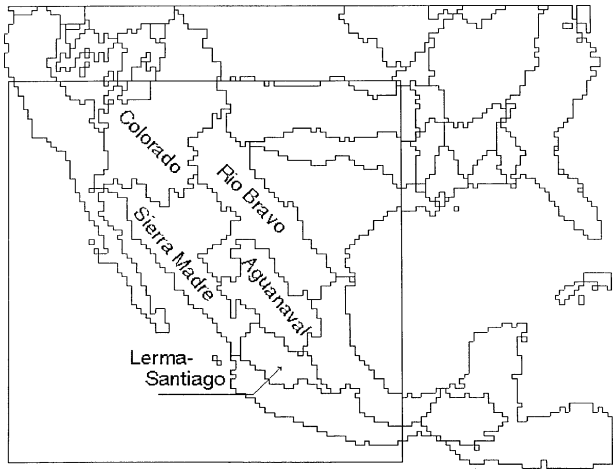

FIG. 2. Basin coverages for basin-average calculations used in this study. Coverage regridded to 30-km resolution. Box denotes the approximate extent of the internal (30 km) MM5 domain. Map extent approximates the boundaries of the 90-km domain.

the results along the northern boundary of the internal domain (the other boundaries are mainly over water).

The model was integrated from 0000 UTC 16 May through 0000 UTC 2 August 1999, with lateral boundary conditions for the coarse domain specified from 6-h analyses from the National Centers for Environmental Prediction–National Center for Atmospheric Research (NCEP–NCAR) reanalysis dataset (Kalnay et al. 1996). Sea surface temperatures (SSTs) were prescribed from the weekly sea surface temperature analyses of Reynolds and Smith (1994). These temperature analyses have a horizontal resolution of 1° and show a reasonable evolution of summertime SST over the northern Gulf of California, with peak summertime temperatures ~29°–30°C.

In all three simulations, subgrid convection in the coarse domain was represented using the Betts–Miller–Janjic CPS. The only difference between the three model simulations was the representation of subgrid convection in the internal (30 km) domain, where the Betts–Miller–Janjic (Betts 1986; Betts and Miller 1986; Janjic 1994), Kain–Fritsch (Kain and Fritsch 1990), and Grell (1993; Grell et al. 1994) CPSs were respectively used. As recognized in G1, the use of different convective schemes in the external and internal domains yields simulated atmospheres with somewhat different thermodynamic structures. Simulations using consistent convective frameworks in both model domains would better isolate the biases of each scheme, but scaling assumptions in the GR and KF convective parameterizations precluded their use at the larger (90 km) grid scale. It should also be noted that the NCEP–NCAR reanalysis data used a simplified Arakawa–Schubert convective scheme (Kalnay et al. 1996), which is similar in structure to the Grell scheme. It is likely that the atmosphere generated by the reanalysis includes bias associated with the convective representation used, which could potentially influence the results of this study.

The land surface parameterization (LSP) used in the MM5 modeling system is important in this study because it represents the hydrologic and energy exchange processes at the land–atmosphere interface. The Oregon State University–NCEP land surface scheme (adapted for application within MM5) was used, and the reader is referred to Chen and Dudhia (2001a,b) for a detailed description of this LSP and verification analyses. In these simulations, the initial status of the soil moisture in the LSP was specified from the NCEP–NCAR reanalysis fields, interpolated to the MM5 grids using the MM5 preprocessors, and the MM5 model was then spun up for 2.5 months. The reader should recognize that NCEP–NCAR reanalyses model uses a different land surface model and that some evolving land surface fields, such as soil moisture, may initially be out of equilibrium with the MM5 LSP. Ideally, the 2.5-month spinup period is sufficient to adequately equilibrate these fields because some hydrometeorological responses, such as the generation of surface runoff, depend on them. However, this was not verified in the present study.

b. Hydrometeorological analyses

The earlier study, G1, presented a suite of analysis products that compared several simulated surface and tropospheric variables with observations. Here, we complement G1 by presenting a hydrometeorologically focused analysis that explores how alternative convective representations alter the land surface hydrologic response of macroscale hydrologic basins defined from the USGS 1:250 000 hydrologic unit coverage (HUC) for North America (USGS 2001). Basins defined in this way were projected onto a 30-km-resolution Lambert conformal coordinate grid to match the grid used in the MM5 simulations.

Figure 2 shows the five so-called level-2 basins used in this study. The selected basins are: the Colorado, Rio Bravo (Rio Grande), Sierra Madre Occidental (SMO), Aguanaval, and Lerma–Santiago (L–S) River basins. They are major hydrologic regions that are under the influence of the NAMS. All basin-relevant calculations were performed in the ArcInfo Geographical Information System (ESRI 2000). Basin-average quantities, including derived quantities such as the convective fraction and the runoff coefficient, are first calculated for each model grid cell and then spatially averaged. In fact, the northernmost portion of the Colorado River basin lies outside of the MM5 model domain (Fig. 2). Omission of part of this basin clearly inhibits comparison between basin-averaged calculations and observations, but it does not greatly affect the results of the present (sensitivity) study. It is also worth noting that the Sierra Madre Occidental basin is not a single watershed; rather,

it is an amalgamation of several basins along the crest of the Sierra Madre cordillera.

1) PRECIPITABLE WATER

The present study extended the precipitable water (PW) analyses given in G1 to include investigation of the change in monthly average PW content between June and July 1999. According to the Tucson National Weather Service office, the onset of the monsoon occurred on 26 June 1999, in Tucson, Arizona. Consequently, the June and July PW results correspond roughly to pre- and postonset values.

2) VERTICALLY INTEGRATED MOISTURE FLUX

Total column-integrated moisture flux **q** can be calculated (Piexoto and Oort 1992) from

$$\mathbf{q} = \frac{1}{g}\int q\mathbf{v}\, dp, \tag{1}$$

where q is specific humidity, $\mathbf{v}$ is the horizontal wind vector, g is the acceleration due to gravity, dp is the thickness of a pressure layer, and the bounds on the integral can be changed to limit the integration to specific levels in the atmosphere. In this study, we chose the integration limits to be between the land surface and the uppermost model layer. Consequently, **q** is the total column-integrated moisture flux. Following Rasmussen (1967), the total water flux at a given level can be partitioned into its time-mean and transient components by

$$\overline{(q\mathbf{v})} = \overline{q}\,\overline{\mathbf{v}} + \overline{q'\mathbf{v}'}, \tag{2a}$$

which, when combined with Eq. (1), gives

$$\mathbf{q} = \frac{1}{g}\left(\int \overline{q}\,\overline{\mathbf{v}}\, dp + \int \overline{q'\mathbf{v}'}\, dp\right). \tag{2b}$$

The left-hand side of Eq. (2b) is the total integrated moisture flux, the first term on the right-hand side is the stationary time-average component, while the second term is the component due to transient eddies. Later, in section 3c, the stationary and transient components of the integrated moisture flux given with each convective scheme are compared.

3) PRECIPITATION CHARACTERISTICS

This study extended the analysis of monthly total rainfall given in G1 to include examination of the partitioning of total monthly precipitation into its convective and nonconvective components. The convective portion of the precipitation occurs whenever the CPS is triggered by environmental conditions, while nonconvective precipitation occurs when saturation occurs at the grid point in the model (Grell et al. 1994). (Interested readers are referred to G1 for an overview of each parameterization and to the relevant references given in section 2a for details.) The relative contribution of convective and nonconvective processes to precipitation for a watershed can be assessed from these components using the convective fraction (CFX), which is calculated by

$$\mathrm{CFX} = \frac{r_c}{(r_c + r_n + \varepsilon)}, \tag{3}$$

where r_c and r_n are the monthly total convective and nonconvective rainfall amounts, respectively, and ε ($=0.001$) is a small term included to ensure that Eq. (3) is defined when there is no rainfall. The basin-average convective fraction values given in Table 1 are calculated as the spatial average of the convective fraction for each grid square in the basin.

The NAMS regime is characterized by a strong diurnal variation in precipitation (Douglas 1995; Negri et al. 1994; Berbery 2001). The diurnal cycle of precipitation was examined by calculating the monthly mean precipitation intensity at each grid point at 3-h intervals (0000, 0300, 0600, 0900, 1200, 1500, 1800, 2100 UTC) for each CPS and importing these values into ArcInfo to calculate the basin-average intensity.

4) SURFACE RUNOFF

The surface runoff calculated by the land surface model in MM5 is part of the standard model output. The formulation adopted by the model (Chen and Dudhia 2001a) is the Simple Water Budget (SWB) method first proposed by Schaake et al. (1996). Surface runoff is the portion of precipitation reaching the ground surface that falls at a rate in excess of the maximum infiltration rate, $I_{\max}$ for the soil. However, $I_{\max}$ is not a fixed value determined by soil type; rather it is a time-varying function of soil water content and precipitation rate. To account for subgrid-scale heterogeneity in soil physical characteristics, a greater fraction of the subgrid area is designated as being saturated as the mean soil moisture increases. Thus, the calculated surface runoff given by the LSP recognizes both infiltration-excess and saturation-excess runoff-generation mechanisms. The subsurface runoff calculated by the LSP is assumed to result only from gravitational percolation. It is estimated from the hydraulic conductivity from the lowest soil layer and consequently varies with soil water content.

The relationship between precipitation and runoff was explored by estimating the runoff coefficient (QFX), that is, the portion of total precipitation that ultimately becomes surface runoff, which is calculated by

$$\mathrm{QFX} = \frac{Q}{P}, \tag{4}$$

where Q is the surface runoff calculated by the LSP for each grid cell and P is the total precipitation for each grid cell (i.e., the sum of the convective and nonconvective portions of precipitation).

TABLE 1. Basin-average precipitation characteristics for NAM macroscale basins shown in Fig. 2. See text for detailed explanation of terms.

Basin/CPS	Precipitation			Convective fraction
	Total (mm)	Convective (mm)	Nonconvective (mm)	
Colorado River				
BM	27.9	24.7	3.2	0.53
KF	56.2	41.2	14.9	0.67
GR	5.6	4.8	0.8	0.82
Sierra Madre Occidental				
BM	239.8	236.0	3.7	0.92
KF	196.1	163.7	32.5	0.86
GR	91.0	61.4	29.6	0.83
Rio Bravo				
BM	19.8	17.7	2.2	0.58
KF	87.1	80.8	6.3	0.96
GR	11.8	10.7	1.2	0.88
Central Mexico—Aguanaval				
BM	46.4	43.2	3.2	0.84
KF	103.7	97.4	6.3	0.95
GR	16.5	11.3	5.1	0.82
Lerma–Santiago				
BM	214.6	207.7	6.9	0.97
KF	203.1	168.1	35.0	0.84
GR	90.6	41.6	49.0	0.53

3. Results

a. Precipitable water

In G1, it was suggested that differences in the modeled low-level wind fields over western Mexico and the Gulf of California were mainly responsible for the differences in the July 1999 monthly average, column-integrated precipitable water fields (see Fig. 3 in G1). Here, this hypothesis is explored further by examining the elements of the atmospheric water balance, that is, the modeled evolution of precipitable water, surface inputs, and the decomposed moisture fluxes.

Figures 3a,c,e show the change in PW from 1 July to 1 August for the BMJ, KF, and GR simulations, respectively. All three simulations show similar monthly mean PW fields for June 1999 (not shown), but there are differences in the mean fields for July when regional convection is a dominant feature. The integrated moisture content is generally 5–10 mm greater in the simulation made with the KF scheme than with the BMJ and the GR schemes (see G1). In particular, simulations with the BMJ and GR schemes both result in lower PW values than with the KF scheme across the northern regions of the NAM (in Arizona and New Mexico) and the drier interior regions of central Mexico and southern Texas.

The change in PW during July (Figs. 3a,c,e) reveals widespread moistening of the atmosphere in the eastern Pacific in all three simulations. However, there are large differences between the simulations in the Gulf of California and over surrounding land areas. The KF simulation shows the most dramatic moistening, with increases of PW greater than 25 mm in Guaymas Bay. There are widespread increases in PW ($>$10 mm) over much of Arizona and western New Mexico and more moderate increases (5–10 mm) over the central Mexican plateau. Although the simulation with the BMJ scheme produces fairly similar spatial distributions of PW, calculated increases are generally about 5 mm less than with the KF scheme except in eastern portions of the interior domain. The simulation using the GR scheme exhibits the smallest change in PW. Changes in excess of 15 mm are limited to regions south of the U.S.–Mexico border, mainly west of the Sierra Madre Occidental (SMO).

Basin-average changes in precipitable water, *d*PW, for July 1999 are given in Table 2. The KF scheme gives the most atmospheric moistening for all basins except the Lerma–Santiago (L–S) River basin in southern Mexico. Differences in *d*PW in excess of 50% occur between simulations for the Colorado, Rio Bravo, Aguanaval, and L–S River basins. For all basins except the L–S River basin, basin-average increases in *d*PW are lowest for the simulation with the GR scheme.

b. Regional source/sink analyses

Figures 3b,d,f show the average value of the evaporation minus precipitation ($E - P$) term for July 1999. The land surface tends to act as a sink of moisture over the high rainfall areas of the SMO and across much of southern Mexico in all simulations. However, there are

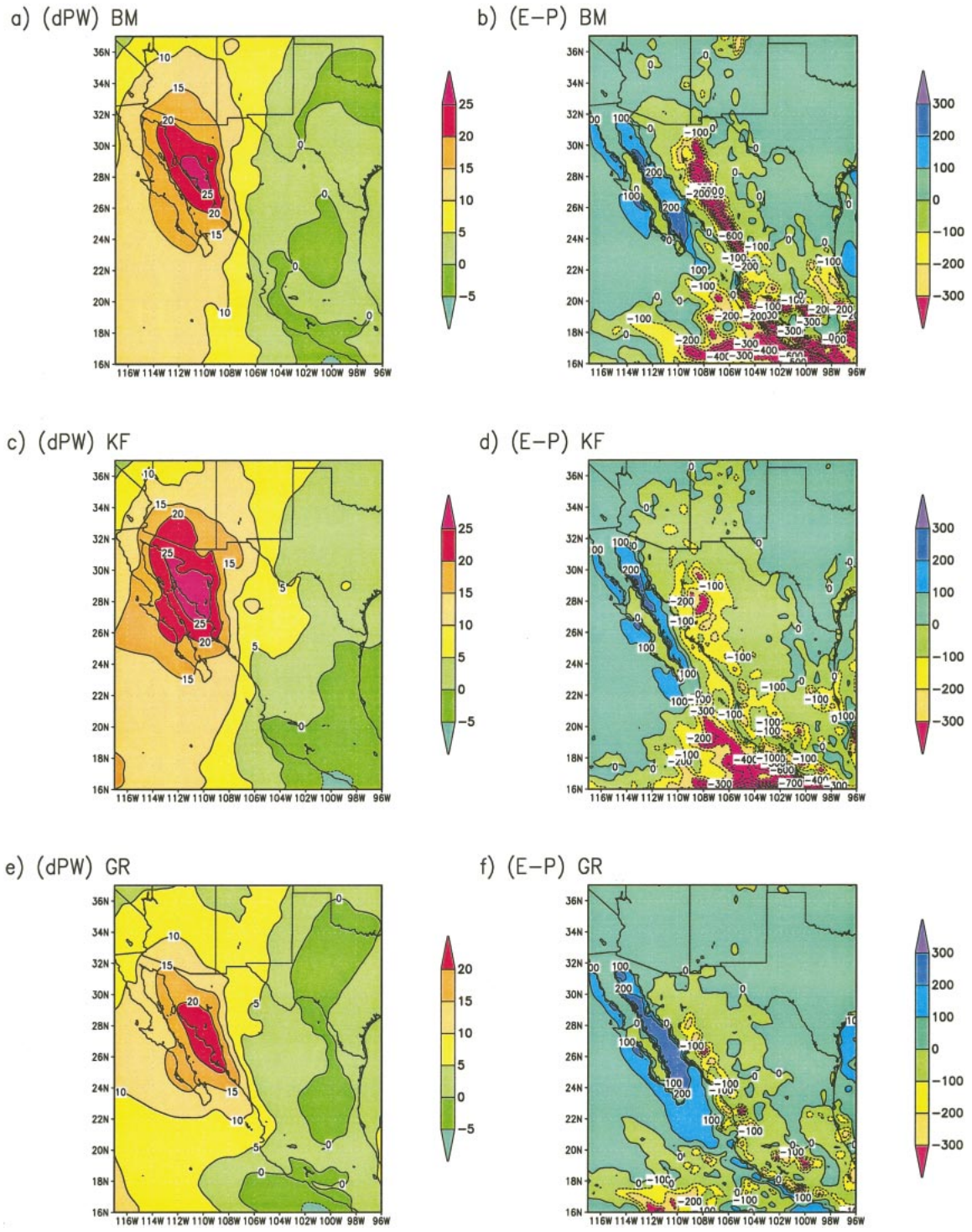

FIG. 3. Change in monthly mean (Jul–Jun), column-integrated precipitable water content [dPW: (a) BMJ, (c) KF, and (e) GR] and the net ($E - P$) source/sink ($\pm$) calculated as Jul monthly evaporation minus Jul monthly total precipitation [$E - P$: (b) BMJ, (d) KF, and (f) GR]. All units are mm. (Note: the zero contour is provided.)

Table 2. Basin-average change in atmospheric water vapor and $E - P$ source/sink for NAM macroscale basins. All values represent basin-average estimates calculated over the regions labeled in Fig. 2. All units are mm.

Basin/CPS	dPW (mm)	$E - P$ (mm)
Colorado River		
BM	10.8	−1.9
KF	12.4	−13.1
GR	6.7	11.1
Sierra Madre Occidental		
BM	12.9	−155.3
KF	15.4	−105.1
GR	11.8	−43.1
Rio Bravo		
BM	3.4	5.1
KF	6.1	−12.5
GR	2.7	10.6
Central Mexico—Aguanaval		
BM	0.6	−10.6
KF	3.9	−25.8
GR	0.8	2.8
Lerma–Santiago		
BM	0.3	−111.7
KF	0.9	−96.0
GR	1.2	−35.6

distinct differences in the magnitudes of the sink between the simulations in some regions. For example, in the simulation with the BMJ scheme, there is a very large sink (corresponding to heavy rainfall) over the SMO. (In G1, it was noted that the BMJ and, to a lesser degree, the KF simulations both overestimated rainfall relative to observations in this region and in southern Mexico.) The broader spatial extent of rainfall given in the KF simulation results in a more widespread land-surface sink than the BMJ and the GR simulations. At times, the signs of the sinks differ; note, in particular, the results for GR simulation in the southwest United States and central Mexico. All three simulations calculate positive ($E - P$) estimates over the Gulf of California, but the GR simulation locates its strongest source there, likely because the simulation with the GR scheme calculates lower atmospheric humidity in the northern Gulf of California than the other simulations.

There are also changes in sign in the basin-average values of the ($E - P$) source/sink given in Table 2. The KF simulation calculates a negative basin-average sink for all basins, while the BMJ simulation calculates the Rio Bravo basin to be a source of atmospheric moisture. However, the GR simulation calculates the inland Colorado, Rio Bravo, and Aguanaval River basins as all being sources of atmospheric moisture. The SMO and L–S River basins are sinks in all simulations, but there are large differences in magnitude. These likely, in turn, affect the behavior of the convective parameterization.

c. Moisture flux components

The vertically integrated stationary and transient eddy moisture flux fields are shown in Fig. 4. In all three simulations (Figs. 4a,c,e), the dominant feature in the stationary component field is the Great Plains low-level jet stream, with moisture fluxes around 300 kg m s^{-1}. Moisture fluxes over the central Mexican plateau have a westward component and are typically less than 90 kg m s^{-1}, indicating that a comparatively small component of the moisture flux emanated from the Gulf of Mexico and crossed this plateau during July 1999. [Note: this feature has also been found in the recent analyses by Berbery (2001), Anderson and Roads (2001), and Stensrud et al. (1995).] The largest differences between simulations are along the coast of western Mexico. Both the KF and BMJ simulations yield southeasterly fluxes up the axis of the Gulf of California that originate well south of the Gulf. This result compares well with field measurements taken during the Southwest Area Monsoon Project in 1990 (Douglas 1995) and the modeling study by Anderson et al. (2000b). These fluxes proceed northward into the low deserts of Arizona and northwestern Mexico. However, the simulation using the GR scheme produces a markedly different result in this region: moisture is transported with a much stronger westward component towards the Pacific Ocean. When the integrated flux was separated into low-level (surface–700 mb) and upper-level (700–400 mb) components (not shown), most of the northward component of the integrated flux was at low levels, while much of the westward component was at high levels. In the GR simulation, mean fluxes across the Gulf of California are quite small and show little directional coherence, although taking monthly average moisture flux fields may mask some of the true behavior in this region because of diurnal variability (Berbery 2001).

As found by Berbery (2001), in this study, the transient moisture flux fields (Figs. 3b,d,f) are generally an order of magnitude less than their stationary counterparts in most regions, but this is not the case over the Gulf of California and the eastern Pacific Ocean. In the eastern Pacific, the transient flux is a substantial portion of the total flux regardless of the CPS used. However, there are notable differences in the modeled transient flux fields and in the way in which transient features are represented. In this region, tropical storms, easterly propagating waves, and, to a lesser degree, midlatitude (short) waves all likely contribute to the mean transient flux (Schmitz and Mullen 1996; Anderson et al. 2000a), and the simulations with alternative convective schemes differ in their representation of such features. Over the Gulf of California, the direction of the transient flux component is northwest in all three schemes, indicating that transient features carry moisture away from the core monsoon region over the Sierra Madre Occidental. With all convective schemes, transient fluxes are negligible across most of central Mexico and have a northeastward

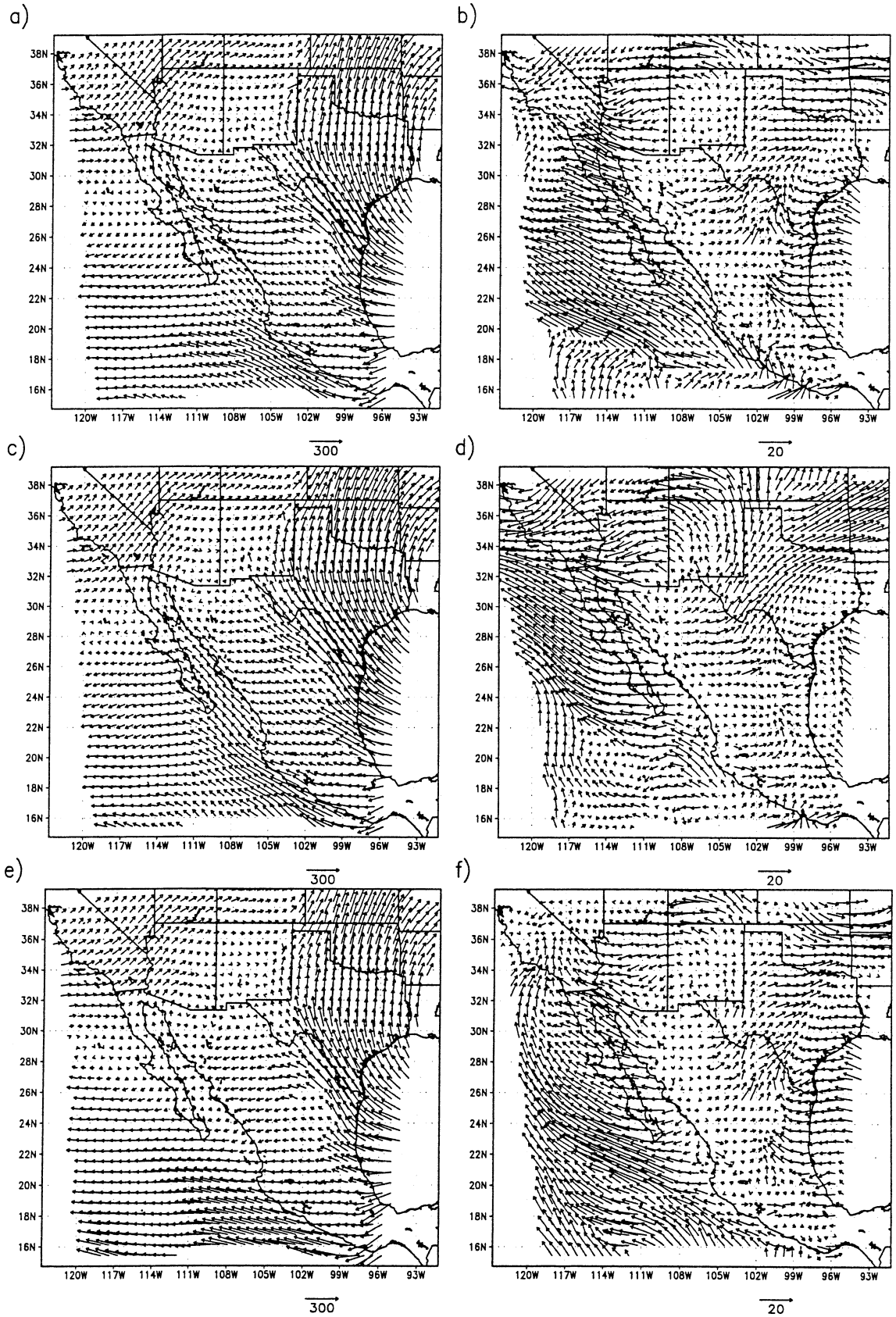

FIG. 4. Jul stationary component [(a) BMJ, (c) KF, and (e) GR] and transient component of the column-integrated moisture flux [(b) BMJ, (d) KF, and (f) GR]. Units are kg m s^{-1}.

component in northeastern Mexico, indicating it is unlikely that significant moisture is transported by transients westward from the Gulf of Mexico into the core monsoon region. However, in all simulations, especially the KF simulation, transient moisture fluxes over Arizona have a marked westward component from New Mexico, suggesting that transient activity may transport moisture into Arizona that originated in the Gulf of Mexico. Further modeling studies which include diagnostic or prognostic tracer routines are needed to test this hypothesis.

d. Precipitation characteristics

July total precipitation and July convective fraction (CFX) are shown in Figs. 5a–f. Errors in the total precipitation fields relative to surface observations were discussed in G1 (see Table 3 in G1). Here, we focus on the regional dependency of convective fraction. It is evident from Figs. 5b,d,f that convective processes influence modeled precipitation across much of the domain in all of the simulations. However, there are marked subregional differences that potentially have important consequences for hydrologic response.

Basin-average values of total, convective, and nonconvective precipitation and CFX are given in Table 1. Over the Colorado River basin, the CFX ranges from 0.53 for the BMJ simulation to 0.82 for the GR simulation. Although it generates the highest convective fraction, using the GR scheme gives the lowest total precipitation (both convective and nonconvective) on a basin-average basis, 10% of that simulated using KF and less than 20% of that simulated using BMJ. (The marked underestimation of precipitation by both the GR and BMJ schemes was noted in G1.) The low convective rainfall indicates that the GR convective schemes is not triggered as frequently as either the BMJ or KF scheme in this northernmost region. Similar behavior occurs over the Rio Bravo basin, although in this case the KF scheme produces much more convective (and hence total) precipitation than either the BMJ or GR schemes.

In the core monsoon region (the SMO), a large amount of convective precipitation occurs with all schemes. As noted in G1, both the BMJ and KF schemes overestimated precipitation in this region compared with observations, while the GR scheme shows only a modest underestimation. It is interesting to note that the spatial variation in total precipitation along the high topography of the SMO is quite large when the BMJ and GR schemes are used but is less when the KF scheme is used. This feature has important consequences for basin-averaged rainfall–runoff processes, as discussed later. In general, convective fraction is quite high throughout the SMO basin, indicating frequent and sustained convective activity with the KF and BMJ schemes, while the GR scheme generates decreasing CFX southward along the coast (Fig. 5f).

The GR simulation (Fig. 5f) shows comparatively low values of CFX over much of southern Mexico, which contributes to the low basin-average value (0.53) for the L–S basin. Nonconvective precipitation over the L–S basin is higher when using the GR scheme, while the BMJ-and, to a lesser degree, KF schemes maintain comparatively high values of CFX across southern and south-central Mexico. Although using the KF scheme generates the most precipitation and highest value of CFX in the Aguanaval basin, using the BMJ scheme generates the highest basin-averaged values in the L–S basin.

In summary, use of the KF scheme generates the most widespread rainfall, most of which is convective in nature. When active, the BMJ scheme tends to produce excessive amounts of convective rainfall compared to the other schemes (and compared to observations, see G1), but very little nonconvective rainfall is generated by this scheme. The GR simulation produces comparatively less precipitation in the northern and inland regions of the NAMS. Although the modeled convective fraction given by the GR scheme is high in these regions, this scheme does not generate sufficient basin-average convective rainfall when compared to observations (and the other schemes). In regions where substantial precipitation is generated using the GR scheme, there is a concomitant increase in nonconvective precipitation, indicating that these environments are persistently moist and that they are likely regions with sufficient moisture convergence to support both convective and nonconvective precipitation.

The diurnal cycle of basin-average total precipitation intensity from each simulation is shown in Fig. 6. Some of the basin-to-basin differences in peak intensity times relate to differences in local solar time, but there is evident sensitivity of the timing and intensity to the convective parameterization used in the simulation. The northernmost basins, the Colorado and Rio Bravo River basins, and the inland basin of the Agaunaval River all show depressed diurnal cycles relative to those in the SMO and L–S River basins. Table 3 shows that using the KF convective parameterization generates both the highest mean intensity and the maximum rainfall intensity in northern and inland regions. The hypothesis (posed in G1) that the KF scheme triggers more frequently than the BMJ or GR schemes is supported because convective rainfall in these northern regions is substantially greater than nonconvective rainfall. In a similar vein, the KF simulation generates rainfall earlier in the day in all regions, indicating that its convective trigger is activated at a comparatively lower threshold.

In the core region of the monsoon (the SMO) and the L–S River basin, there are marked increases in modeled precipitation intensity during afternoon hours with all schemes, but the peak intensity occurs 3–6 h earlier with the KF scheme than with the BMJ or GR schemes. Although the KF simulation generates intense precipitation earlier in the day than the other two schemes, the BMJ scheme generates the highest intensity, 0.60 and

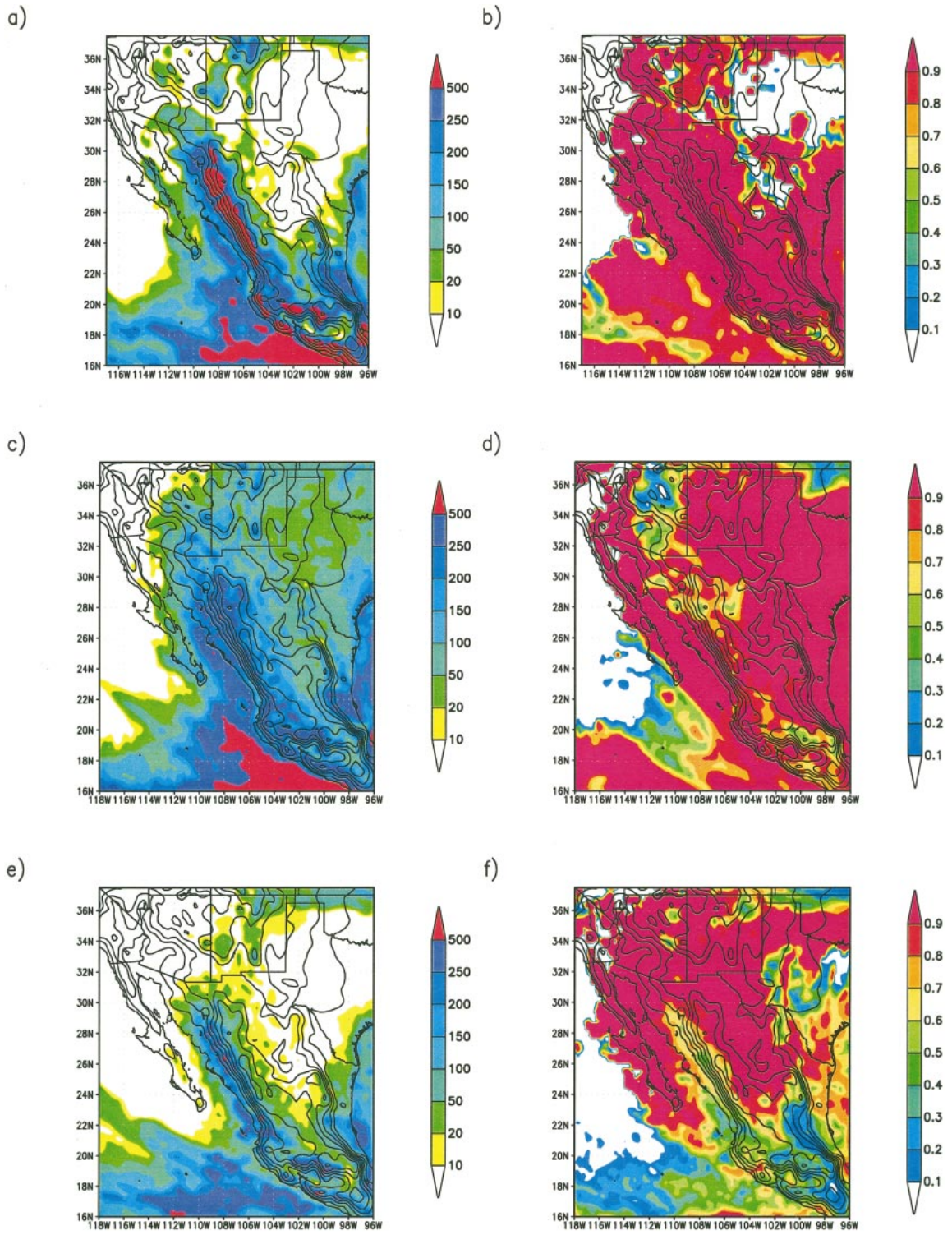

FIG. 5. Jul total precipitation [(a) BMJ, (c) KF, and (e) GR; units are mm] and total convective fraction [(b) BMJ, (d) KF, and (f) GR; dimensionless].

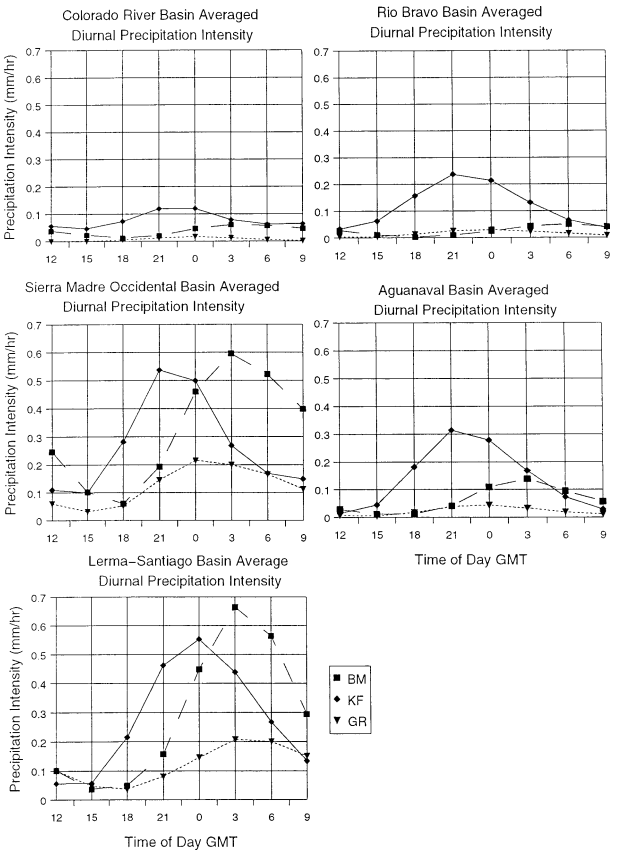

FIG. 6. Basin-averaged, Jul mean diurnal precipitation intensity. Units are mm h^{-1}.

0.66 mm h^{-1} for the SMO and L–S basins, respectively. This is consistent with the result (from G1) that the BMJ and, to a lesser degree, the KF schemes tend to overpredict rainfall in these two regions.

With the GR scheme, the diurnal cycle is notably depressed in amplitude compared to the KF or BMJ schemes, about 3 times less in the river basins most affected by the monsoon (SMO and L–S). Two factors contribute to this. First, a larger portion of the precipitation falling in these basins in nonconvective: convective fractions for the SMO and L–S River basins when using the GR scheme were 0.83 and 0.53, respectively; compared to 0.86 and 0.84, respectively, for the KF scheme; and 0.92 and 0.97, respectively, for the BMJ scheme. Second, the strong spatial gradients in total precipitation given with the GR scheme means that, in basin-average calculations, the widespread areas of low precipitation act to smooth the maximum precipitation intensity, which is localized along the western slope of the SMO. Similar compensation likely occurs in the case of the BMJ simulation, but the strength of SMO rainfall with the BMJ scheme dominates. The differing precipitation amount, timing, and intensities of rainfall in the simulations impact the generation of modeled runoff from basins, as discussed later.

Although basin-average calculations are helpful when investigating the sensitivity of regional hydroclimatology to model parameterization, aspects of the hydrologic cycle may not be adequately captured because of the spatial averaging across the basin. In fact, as shown in the next section, spatial gradients in precipitation have an important influence on basin-average statistics and runoff generation processes. These are masked when precipitation amount and intensity are averaged across large basins. Temporal averaging also acts to smooth precipitation intensity. None of the rainfall intensities given in Fig. 6 and in Table 3, for instance, are likely to generate appreciable amounts of surface runoff. Addressing these problems is the core issue in hydrologic scaling as discussed theoretically by Wood et al. (1988) and is the subject of our ongoing research.

e. Surface and subsurface runoff

Basin-average and maximum total precipitation and modeled surface runoff are tabulated in Table 4 along with basin-average values of the runoff coefficient, QFX. Values of QFX are very low (1%–3%) with all convection schemes and in all basins, except for the SMO basin, indicating that, as a spatial average, precipitation rate rarely exceeds the local infiltration capacity. However, on a local (or gridpoint) basis, this is not the case. The simulation with the BMJ scheme generates the highest runoff coefficients in the Rio Bravo and Aguanaval basins, and results in similar values as the KF and GR schemes in the Colorado and L–S basins respectively. On the other hand, the GR scheme gen-

TABLE 3. Basin-average, monthly mean diurnal precipitation intensity (mm h^{-1}) for NAM macroscale basins. Bold text indicates maximum value of the three simulations.

	BM		KF		GR	
	Mean	Max	Mean	Max	Mean	Max
Basin						
Colorado	0.04	0.06	**0.08**	**0.12**	0.01	0.02
Rio Bravo	0.03	0.05	**0.12**	**0.24**	0.02	0.03
Sierra Madre Occidental	**0.32**	**0.60**	0.26	0.54	0.12	0.22
Aguanaval	0.06	0.14	**0.14**	**0.31**	0.02	0.04
Lerma–Santiago	**0.29**	**0.66**	0.27	0.55	0.12	0.21
Ranges (all schemes)	Mean	0.01–0.32		Max	0.02–0.66	

TABLE 4. Basin-average rainfall–runoff characteristics for NAM macroscale basins shown in Fig. 2. Max columns indicate gridpoint maximum values for the respective basin and simulation. See text for detailed explanation of terms.

Basin/CPS	Total precipitation (mm)	Max total precipitation (mm)	Surface runoff (mm)	Max surface runoff (mm)	Surface runoff ratio (QFX)	Deep drainage (mm)	Max deep drainage (mm)	Total runoff (mm)
Colorado River								
BM	27.9	493.2	0.9	34.0	0.01	3.9	226.3	4.8
KF	56.2	274.5	0.8	17.7	0.01	3.0	42.6	3.8
GR	5.6	81.5	0.0	1.3	0.00	2.9	20.5	2.9
Sierra Madre Occidental								
BM	239.8	972.0	21.5	278.6	0.05	10.4	332.4	31.9
KF	196.1	531.3	6.4	60.4	0.03	0.3	97.5	6.7
GR	91.0	583.6	15.9	225.6	0.08	0.2	94.3	16.1
Rio Bravo								
BM	19.8	360.0	0.7	22.0	0.02	0.7	93.3	1.5
KF	87.1	332.7	1.2	7.7	0.01	0.3	21.1	1.5
GR	11.8	126.6	0.1	1.9	0.00	0.3	13.7	0.3
Central Mexico—Aguanaval								
BM	46.4	440.1	1.4	25.4	0.02	0.4	49.2	1.8
KF	103.7	228.9	1.0	7.8	0.01	0.0	1.8	1.0
GR	16.5	117.4	0.2	20.2	0.01	0.0	0.2	0.2
Lerma–Santiago								
BM	214.6	1172.7	11.0	308.7	0.03	19.8	587.5	30.7
KF	203.1	435.0	2.5	33.0	0.01	3.1	142.2	5.7
GR	90.6	402.7	3.8	49.4	0.03	1.1	109.0	5.0

erates the highest value of QFX in the SMO basin. Combining all of the basins, the BMJ scheme gives the highest average surface runoff coefficient (0.03), followed by the GR scheme (0.02), and the KF scheme (0.01). At first sight, this is perplexing because the BMJ and KF schemes generate substantially greater basin-average peak precipitation intensity than the GR scheme. In terms of total surface runoff, the BMJ scheme yields most in the Colorado, SMO, Aguanaval, and the L–S River basins, while the KF simulation produces an equal amount in the Rio Bravo basin. Additionally, the GR scheme produces more runoff in the SMO and L–S River basins than the KF scheme, with less total rainfall and less convective rainfall. These results are counterintuitive because basins with the greatest basin-averaged precipitation or the highest basin-averaged rainfall intensity might be expected to generate the greatest surface runoff.

Consider the spatial patterns of runoff shown in Figs. 7a,c,e and QFX given in Figs. 7b,d,f. Consistent with the surface runoff presented in Table 4, local surface runoff with the KF scheme is much less than with either the BMJ or GR schemes in the core monsoon region (the SMO), despite the fact that the KF scheme produces not only both more total and more convective basin-average rainfall than the GR scheme, but also a markedly higher basin-average rainfall intensity (Fig. 6). However, recall that surface runoff is generated in the model (and in reality) only when the local rainfall rate exceeds the local maximum infiltration capacity. The GR simulation calculates locally greater precipitation fall with locally very high rates compared to the KF simulation. This feature is evident along the southern coast of Mexico as well as along the SMO.

There is evidence of these phenomena in Table 4: using the BMJ scheme results in the highest maximum values of both precipitation and surface runoff in every basin. As noted earlier (in section 3e and G1), when the BMJ scheme does generate convective rainfall, it appears it does so at rates well in excess of the other two schemes (and likely in excess of observations). The intensity plots for the SMO and L–S basins (Fig. 6) suggest that much of the precipitation given by the BMJ scheme falls at intense rates but, in other basins, the basin-average rainfall intensity and total precipitation given with the BMJ scheme are moderated by spatial averaging to include large regions with no rainfall. Although the GR scheme produces greater maximum rainfall in the SMO basin than the KF scheme, the difference in surface runoff is not proportional, and more surface runoff is produced in the L–S basin with the GR scheme than with the KF scheme, even though the local maximum precipitation is lower. Thus, the apparently anomalous interrelationship between rainfall and surface runoff is a consequence of averaging rainfall patterns that differ greatly in terms of their local intensity and spatial extent across large basins.

The cumulative mass plot for the two grid cells with the largest surface runoff in the SMO basin with the KF and GR schemes are given in Figs. 8a and 8b, respectively. (Note: These are not at the same location in the two simulations. With the KF scheme, the location

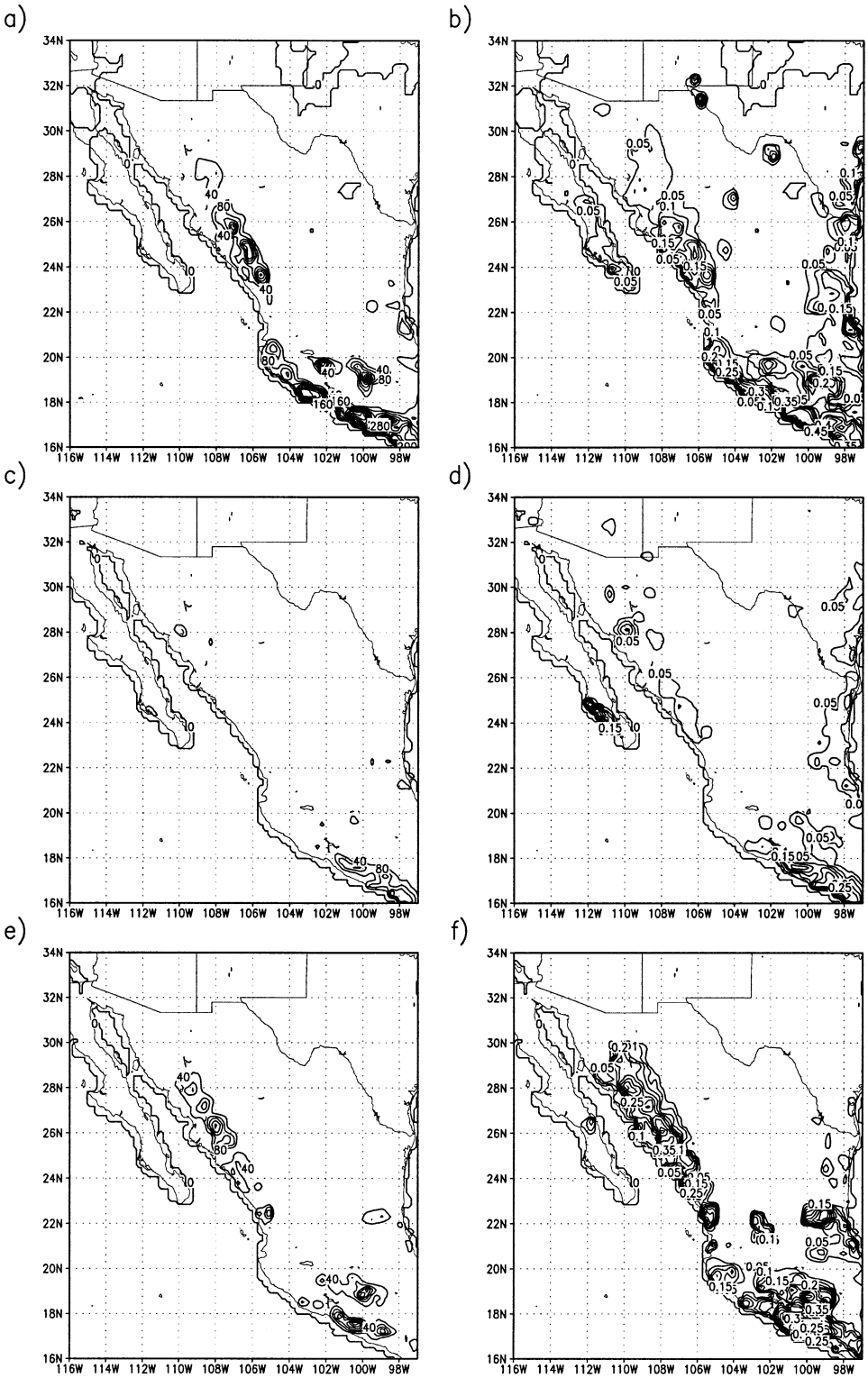

FIG. 7. Jul total surface runoff [(a) BMJ, (c) KF, and (e) GR; units in mm, contour interval is 40 mm] and surface runoff coefficient [(b) BMJ, (d) KF, and (f) GR; dimensionless, contour interval is 0.05].

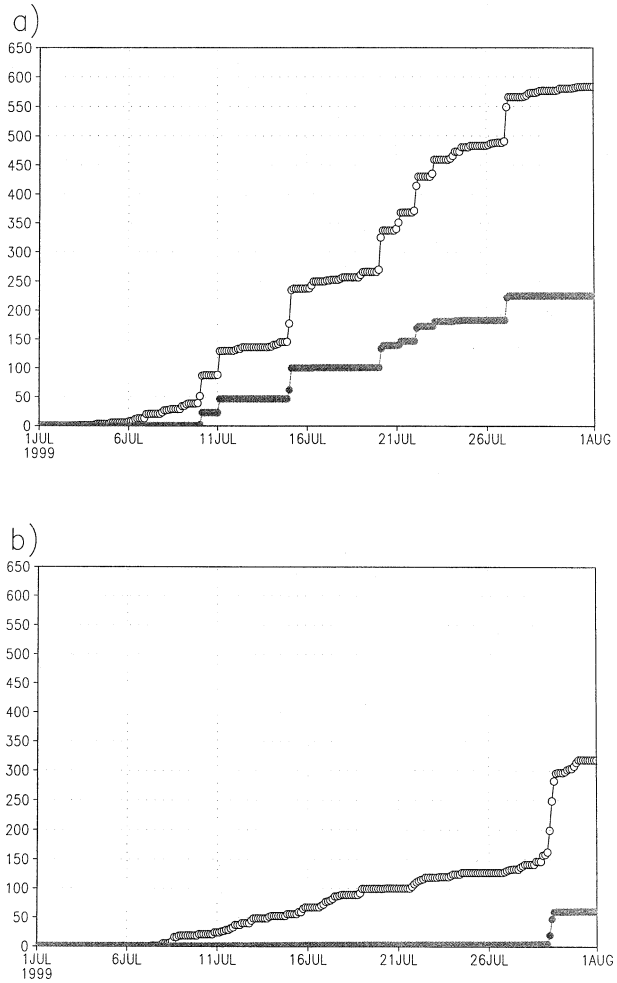

FIG. 8. Cumulative mass curve for precipitation (open circles) and surface runoff (closed circles) at the location of maximum surface runoff in the SMO basin for (a) GR and (b) KF. Units are mm.

with maximum surface runoff is not where the maximum monthly total precipitation occurs. With the GR scheme it is.) In both cases, large increases in surface runoff are correlated with large precipitation events. In the case of the GR simulation (Fig. 8a), three large events (15, 20, and 27 July), each lasting more than 3 h with local rainfall rates greater than or equal to 15 mm h^{-1}, and several other smaller events of shorter duration but near-equal intensity all contribute to the cumulative surface runoff. In the simulation with the KF scheme (Fig. 8b), although there is equally persistent occurrence of precipitation, only one event (29 July) has sufficiently intense precipitation ($\sim$13 mm h^{-1}) to generate surface runoff. This example illustrates a general point. In this region, local precipitation intensity in discrete, local storms plays a more important role in generating local and, subsequently, basin-average surface runoff than does basin-average precipitation amount or basin-average rainfall intensity.

Values of subsurface runoff (or deep drainage) and total runoff are also given in Table 4. In the core monsoon region (SMO), runoff (as calculated by the LSP) is dominated by surface runoff, but deep drainage is equal to or exceeds surface runoff in 7 of the 15 cases (corresponding to three CPSs and five basins). The Colorado River basin, where soil moisture is likely high during spring, is noteworthy in this respect, and the release of winter and springtime moisture may also contribute to comparable surface runoff and deep drainage values in the Rio Bravo basin. High values of deep drainage also occur in the L–S basin, likely due to saturated soils during warm season rains. As with basin-average surface runoff, there is evidence of considerable spatial averaging of deep drainage because basin-maximum values often exceed the basin-average by several orders of magnitude, especially when the BMJ scheme is used. The locations of maxima tend to coincide with the location of large, stationary precipitation events generated by the BMJ scheme.

4. Discussion and conclusions

This study extends the sensitivity analyses in G1 to investigate regional and subregional sensitivities of hydrometeorological and hydrological responses to the convective parameterization used in a regional climate simulation of the North American monsoon. The main conclusions from this study can be summarized as follows:

- The differing evolution of precipitable water fields given with different convective parameterizations in MM5 simulations in July 1999 appear to be related to differences in both the column-integrated moisture flux fields and the strength of the surface source/sink. These differences result in markedly different patterns of convective and nonconvective precipitation.
- As suggested in G1, using the KF scheme produces more widespread convective rainfall than using the BMJ or GR schemes: using the BMJ and GR schemes gives precipitation that is largely in southern Mexico or locked to the topography of the SMO. The BMJ scheme produces comparatively low amounts of nonconvective rainfall but, when triggered, produces comparatively high rates of convective rainfall. The GR scheme consistently produces the lowest amount of convective precipitation.
- There are substantial variations in the magnitude of the $E - P$ source/sink between simulations in different river basins and, in some cases, the sign of the source/sink is reversed. Because the KF scheme generates extensive rainfall coverage, it consistently predicts a surface sink of moisture in all regions. However, using the GR scheme results in a basin-averaged moisture source for all basins except the SMO and the L–S River basins.
- The KF scheme gives the highest basin-average rainfall intensity in the northern and inland basins of the

Colorado, Rio Bravo, and Aguanaval River basins, while the BMJ scheme produces the highest basin-average intensity for the SMO and the L–S River basins. The GR scheme shows a suppressed diurnal cycle in basin-average precipitation intensity relative to the other schemes, in part because the strong spatial gradients in precipitation means there are extensive regions with low precipitation.

- There are large differences in the monthly total surface runoff between simulations that are more closely related to differences in local rainfall intensity than to time-average precipitation amount or basin-average rainfall intensity. With all schemes, the generation of surface runoff depends more on precipitation rates in individual local storms than on monthly total, basin-averaged precipitation.

This study shows that the strong dependence of the modeled regional climate on the convective parameterization used complicates hydrological analyses and prediction, and it hampers the understanding of the role of land-surface feedbacks in the regional climate system during the NAM. The sensitivity found in this study is greater than that found in a similar study by Small (2001), which investigated the effect of artificial soil-moisture anomalies on tropospheric ridge structure and regional precipitation patterns during the NAM. Small (2001) reported changes in regional precipitation patterns on the order of 20%. In the present study, differences in precipitation are several hundreds of percent in some basins. Because land-surface forcing can affect the triggering of convective events through the surface energy balance, it is likely that the results of studies of land-surface sensitivity will be strongly influenced by the CPS used in the model.

On the basis of this study (and G1), it is apparent that hydrometeorological analyses of the NAMS with otherwise similar physically based models will have substantial uncertainty associated with the representation of subgrid convective processes. This uncertainty extends not only to the precipitation generated by the model, but also to the magnitude and distribution of latent heating generated by the moist convection, which is itself an important influence on the regional circulation (Barlow et al. 1998). The character and origin of the precipitation, its frequency of occurrence, and, of particular importance in hydrological investigations, the intensity of individual storms events, will also be in question.

A shortcoming of the present study is that no calibration of the parameters used in the CPSs or the LSP was attempted. Several major obstacles inhibit model calibration: some pertaining to CPSs were discussed in G1. None of the convective schemes used were designed or calibrated in monsoon-type convective environments in regions of complex terrain. The convective schemes used in this study have evolved over many years and have been calibrated with different physics packages (e.g., planetary boundary layer, diffusion, microphysics schemes, etc.), which influence both convective initiation and feedback processes. Ideally, convective schemes should be tested (and perhaps tuned) with several different physics parameterization combinations to better isolate the true response of the climate to convective representation. LSP calibration studies could also be conducted to determine more appropriate parameter values (especially those involved in the computation of infiltration). However, extensive surface data would be required, but these data are currently lacking over much of the area influenced by the NAM.

The conclusions from this study are based on single realizations with each convective parameterization. Although using a consistent set of boundary conditions constrains model solutions, internal chaotic variability occurs within the model. The use of ensemble techniques, where the model is initialized from a variety of starting dates, and perhaps performing integrations for several different years could help eliminate some of the uncertainty associated with model chaotic behavior. As discussed in G1, the three simulations did not differ appreciably for the month of June, which supports the conclusion that convective representation exerts a strong influence in the simulation of convective regional climates. This conclusion would be strengthened (weakened) if the ensemble mean with a variety of different starting dates and in different years showed similar (different) responses.

Notwithstanding these shortcomings, it is clear from the present study that hydrological fluxes in the semiarid region of the NAM show marked seasonality, with activity highest during the summer months of June–September increasing southwards into Mexico. The climatic variations, and their hydrologic responses that generate floods and challenge water resource managers in the region of southwest North America, are not well understood due to the lack of a sufficiently dense, long-term instrumentation network in this sparsely populated region (Magana and Conde 2000). Lack of high-quality data also complicates the problem of model assessment, verification, and calibration. Hence, while models can currently estimate the range of hydrological responses to variability in the NAM climate, the increased understanding through quantitative assessment and increased predictability await implementation of an enhanced regional observation network such as that proposed for the North American Monsoon Experiment (NAME 2001).

Acknowledgments. Primary support for this study was from NASA Grant NAG5-7554. Additional support came from NOAA Grant NA16GP2002. The authors also wish to thank Dr. Ken Mitchell for his thorough critique of this work and three anonymous reviewers whose comments greatly improved its clarity.

REFERENCES

Anderson, B. T., and J. O. Roads, 2001: Summertime moisture divergence over the southwestern U.S. and northwestern Mexico. *Geophys. Res. Lett.,* **28,** 1973–1976.

——, ——, and S. C. Chen, 2000a: Large-scale forcing of summertime monsoon surges over the Gulf of California and the southwestern United States. *J. Geophys. Res.,* **105** (D19), 24 455–24 467.

——, ——, ——, and H.-M. Juang, 2000b: Regional simulation of the low-level monsoon winds over the Gulf of California and southwestern United States. *J. Geophys. Res.,* **105** (D14), 17 955–17 969.

BANDAS, 1998: Bancos Nacional de Datos de Aguas Superficiales. Comission Nacional del Agua (can) y Instituto Mexicano de Tecnologia del Agua (IMTA), CD-ROM.

Barlow, M., S. Nigam, and E. H. Berbery, 1998: Evolution of the North American monsoon system. *J. Climate,* **11,** 2238–2257.

Berbery, E. H., 2001: Mesoscale moisture analysis of the North American monsoon. *J. Climate,* **14,** 121–137.

Betts, A. K., 1986: A new convective adjustment scheme, I: Observational and theoretical basis. *Quart. J. Roy. Meteor. Soc.,* **112,** 677–691.

——, and M. J. Miller, 1986: A new convective adjustment scheme, II: Single column tests using GATE wave, BOMEX, ATEX, and arctic air-mass data sets. *Quart. J. Roy. Meteor. Soc.,* **112,** 693–709.

Chen, F., and J. Dudhia, 2001a: Coupling an advanced land surface–hydrology model with the Penn State–NCAR MM5 modeling system. Part I: Model implementation and sensitivity. *Mon. Wea. Rev.,* **129,** 569–585.

——, and ——, 2001b: Coupling an advanced land surface–hydrology model with the Penn State–NCAR MM5 modeling system. Part II: Preliminary model validation. *Mon. Wea. Rev.,* **129,** 587–604.

Douglas, M. W., 1995: The summertime low-level jet over the Gulf of California. *Mon. Wea. Rev.,* **123,** 2334–2347.

ESRI, 2000: ARC/INFO Version 8.0. Environmental Systems Research Institute, Inc.

Giorgi, F., and L. O. Meams, 1999: Introduction to special section: Regional climate modeling revisited. *J. Geophys. Res.,* **104** (D6), 6335–6352.

Gochis, D. J., W. J. Shuttleworth, and Z.-L. Yang, 2002: Sensitivity of the modeled North American monsoon regional climate to convective parameterization. *Mon. Wea. Rev.,* **130,** 1282–1298.

Grell, G. A., 1993: Prognostic evaluation of assumptions used by cumulus parameterizations. *Mon. Wea. Rev.,* **121,** 764–787.

——, J. Dudhia, and D. R. Stauffer, 1994: A description of the fifth-generation Penn State/NCAR Mesoscale Model (MM5). NCAR Tech. Note NCAR/TN-380+STR, 138 p.

Higgins, R. W., Y. Yao, and X.-L. Wang, 1997: Influence of the North American Monsoon system on the U.S. summer precipitation regime. *J. Climate,* **10,** 2600–2622.

Janjic, Z. I., 1994: The step-mountain eta coordinate model: further developments of the convection, viscous sublayer, and turbulence closure schemes. *Mon. Wea. Rev.,* **122,** 927–945.

Kain, J. S., and M. Fritsch, 1990: A one-dimensional entraining/detraining plume model and its application in convective parameterization. *J. Atmos. Sci.,* **47,** 2784–2802.

Kalnay, E., and Coauthors, 1996: The NCEP/NCAR 40-Year Reanalysis Project. *Bull. Amer. Meteor. Soc.,* **77,** 437–471.

Magana, V. O., and C. Conde, 2000: Climate and freshwater resources in northern Mexico: Sonora, a case study. *Environ. Monit. Assess.,* **61,** 167–185.

Morehouse, B. J., R. H. Carter, and T. W. Sprouse, 2000: The implications of sustained drought for transboundary water management in Nogales, Arizona and Nogales, Sonora. *Nat. Resour. J.,* **40,** 783–817.

NAME, cited 2001: North American Monsoon Experiment science plan. [Available online at http://yao.wwb.noaa.gov/monsoon/NAME.html.]

Negri, A. J., R. F. Adler, E. J. Nelkin, and G. J. Huffman, 1994: Regional rainfall climatologies derived from Special Sensor Microwave Imager (SSM/I) data. *Bull. Amer. Meteor. Soc.,* **75,** 1165–1182.

Peixoto, J. P., and A. H. Oort, 1992: *Physics of Climate.* American Institute of Physics, 520 pp.

Rasmussen, E. M., 1967: Atmospheric water vapor transport and the water balance of North America. Part 1. Characteristics of the water vapor flux field. *Mon. Wea. Rev.,* **95,** 403–426.

Reynolds, R. W., and T. M. Smith, 1994: Improved global sea surface temperature analyses. *J. Climate,* **7,** 929–948.

Schaake, J. C., V. I. Koren, Q. Y. Duan, K. Mitchell, and F. Chen, 1996: Simple water balance model for estimating runoff at different spatial and temporal scales. *J. Geophys. Res.,* **101** (D3), 7461–7475.

Schmitz, J. T., and S. L. Mullen, 1996: Water vapor transport associated with the summertime North American monsoon as depicted by ECMWF analyses. *J. Climate,* **9,** 1621–1634.

Small, E. E., 2001: The influence of soil moisture anomalies on variability of the North American monsoon system. *Geophys. Res. Lett.,* **28,** 139–142.

Stensrud, D. J., R. L. Gall, S. L. Mullen, and K. W. Howard, 1995: Model climatology of the Mexican monsoon. *J. Climate,* **8,** 1775–1794.

USGS, cited 2001: Digital coverage archive. [Available online at http://water.usgs.gov/GIS/metadata/usgswrd/huc250k.html.]

Wood, E. F., M. Sivapalan, K. Beven, and L. Band, 1988: Effects of spatial variability and scale with implications to hydrologic modeling. *J. Hydrol.,* **102,** 29–47.